PROCEEDINGS OF SCIENCE

Calibration of the Radio Neutrino Observatory in Greenland using thermal noise

The RNO-G Collaboration
(a complete list of authors can be found at the end of the proceedings)

E-mail: ruben.camphyn@ulb.be

The Radio Neutrino Observatory in Greenland (RNO-G) aims to detect ultra-high-energy astrophysical neutrinos (E > 100 PeV). These neutrinos interact with the Greenlandic ice sheet, generating a particle cascade that emits radiation in the radio frequency range through the Askaryan effect. Once fully deployed, RNO-G will be the largest in-ice radio neutrino detector. Currently, 8 out of 35 planned detector stations have been built and are actively collecting science data.
This work aims to perform an end-to-end in-situ absolute amplitude calibration using randomly triggered data, filtered to only include thermal noise background. Precise understanding of the absolute system gain is essential for interpreting RNO-G's science data. Moreover, an accurate knowledge of the system response is key to optimize detector simulation, hence enhancing the reliability of analysis outcomes. To this end, thermal noise is simulated by taking into account both electronic noise and thermal radiation from the surrounding ice, folded through a nominal detector description of the instrument response as measured in the lab. By comparing simulated noise and detected noise, a calibration has been derived to fine-tune the description of the absolute system gain.

Corresponding authors: Camphyn R.[1,2*], Schlüter F.[1], Toscano S.[1]

[1] *Université Libre de Bruxelles - Inter-University Institute For High Energies*

[2] *Fonds de la Recherche Scientifique*

[*] Presenter

39th International Cosmic Ray Conference (ICRC2025)
15–24 July 2025
Geneva, Switzerland

© Copyright owned by the author(s) under the terms of the Creative Commons Attribution-NonCommercial-NoDerivatives 4.0 International License (CC BY-NC-ND 4.0).

PoS(ICRC2025)1003

1. Introduction

The Radio Neutrino Observatory in Greenland (RNO-G) [1] is a next-generation radio neutrino detector that aims to detect the traces of cosmic neutrinos arriving at Earth. Incoming neutrinos can interact with the natural ice in which the detector is built and initiate a particle cascade that emits radio frequency radiation due to the Askaryan effect [2]. The main science goal is to characterize the astrophysical neutrino spectrum to energies at or above $E \geq 100$ PeV. RNO-G's results are expected to lead to the detection of a high energy neutrino source, detection of the cosmogenic neutrino flux or improved limits on models for both [3].

To accurately interpret recorded data, a fine-tuned knowledge of the detector's system response is necessary. This analysis aims to provide an in-situ calibration of the absolute amplitude of the system response using randomly triggered data.

2. Calibration strategy

The absolute amplitude calibration is performed by comparing the average frequency spectra of thermal noise data S_{obs} with simulation. The simulation consists of spectra calculated from proposed thermal noise sources S_{noise} combined with a normalized system response measurement $\hat{H}_{\text{system}}$. The response is scaled by an **absolute** system gain G to obtain maximum agreement between simulation and data:

$$S_{\text{obs}}(f) = G \cdot \hat{H}_{\text{system}}(f) \cdot S_{\text{noise}}(f), \tag{1}$$

in which f denotes frequency. The result is the calibrated system response $H_{\text{system}} = G \cdot \hat{H}_{\text{system}}$.

After appropriate cleaning, we can assume the data to contain only known thermal noise sources, which are assumed to be: blackbody radiation of the ice surrounding the detector, the instrument's electronic noise and the radio background coming from the Galaxy. We use the `NuRadioMC` framework [4] to simulate these components.

It is important to note that the calibrated system response H_{system} does not include the antennas. The antenna beam patterns and vector effective lengths have been simulated by the RNO-G collaboration [1] and are included in the noise simulation S_{noise}.

In the following sections, we will elaborate more on each of the calibration procedure's aspects. We start with a description of the system, justify the selection of data, describe each simulated component and end with the procedure for obtaining the calibration coefficients.

3. System response and data

Currently under construction in Greenland, the RNO-G array will feature 35 independent stations spaced over an area of ~50 km^2 [1]. Construction started in the summer of 2021 and, at present, 8 stations have been deployed and are taking data. Each station is built on a hybrid design principle, containing both surface antennas placed in shallow trenches (surface component) and instrumented ~100 m deep boreholes (deep component), as shown in Figure 1 (**left**). The deep component contains the main trigger, which consists of four antennas placed in a phased array (PA) setup [5].

PoS(ICRC2025)1003

Three types of antennas are used. First, the phased array consists exclusively of vertically polarized antennas (VPols). Second, the deep component without phased array contains VPols and horizontally polarized antennas (HPols). Third, the surface component contains Log Periodic Dipole antennas (LPDAs) that are either oriented to face upwards to veto cosmic ray backgrounds or downward to aid in event reconstruction.

3.1 System description

We describe the system as the signal chain after the antenna. This system's response is described by our calibrated result H_{system}.

The main components of the system are illustrated in Figure 1 (**right**). The borehole antenna signal is passed through an In-ice Gain with Low-power Unit (IGLU) amplifier, before being transmitted over optical fiber to the DAQ box at the surface, which contains the Downhole Receiver & Amplifier Board (DRAB) amplifier. The signal is then passed over a coaxial cable to be digitized at the main DAQ board, the RAdio DIgitizer and Auxiliary Neutrino Trigger (RADIANT).

The surface antenna signal is not amplified at the antenna but carried by coaxial cable from antenna to the SURFACE amplifier, before also arriving at the RADIANT.

The system response template $\hat{H}_{\text{system}}$ was measured by inserting a sub-ns pulse at the IGLU and recording the result on the RADIANT output. The measurement is normalized such that the maximum gain amplitude is set to 1.

The phased array channels include a signal splitter due to the trigger, which affects the overall system response. As a result, three distinct signal chains can be identified; the phased array; the deep component without phased array, which we refer to as the helper component; and the surface component. The measurements for all three systems are shown in Figure 2.

3.2 Data selection

RNO-G uses a *forced* trigger that initiates data taking every 10 seconds for monitoring the ambient background. In this analysis, we select data from a single station and from the 2023 season, which encompasses the months May through June of 2023. The dataset is cleaned as follows:

A maximum trigger rate of 2 Hz over 2 hour data taking runs is imposed to remove very noisy periods such as windy periods or anthropogenic activity.

A continuous wave filter is applied to limit e.g. anthropogenic noise such as a monitoring weather balloon over Summit station that emits a radio signal at 403 MHz.

A digital Butterworth bandpass filter of order 10 with a bandwidth of $100-700$ MHz is applied to select data within the antenna effective bandwidth.

Figure 3 shows the average frequency spectrum for one of the PA antennas obtained after the cleaning procedure. The spectrum contains ~400000 time traces of 600 ns each.

4. Thermal noise simulations

A thermal noise simulation is created by working in a bottom-up approach. The physical components visible in data are identified and simulated independently:

PoS(ICRC2025)1003

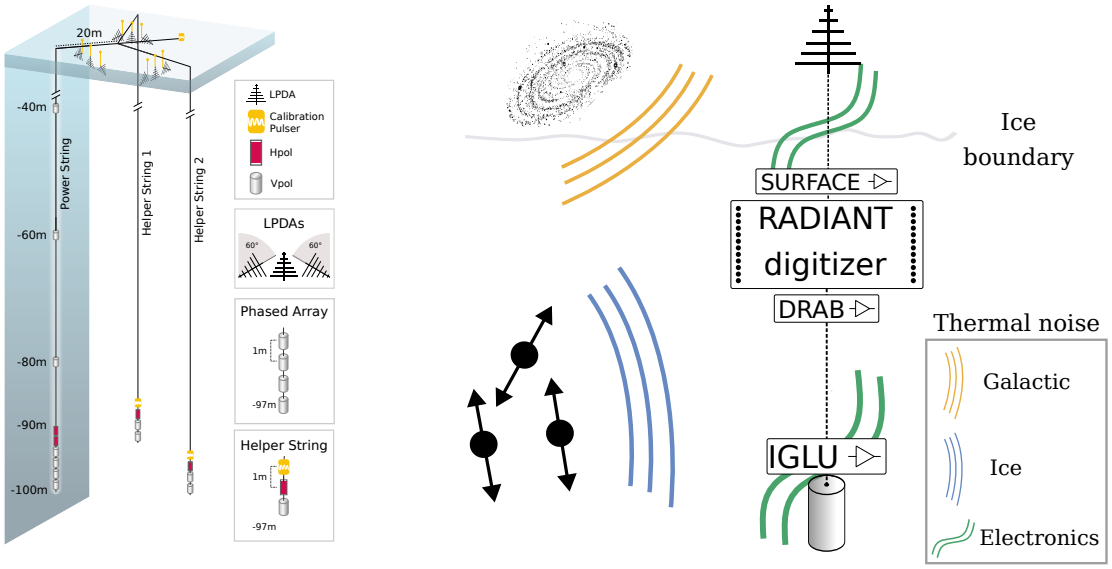

Figure 1: Left Schematic of a single station as installed for the first seven RNO-G stations, showing the hybrid design of shallow antennas and instrumented boreholes. **Right** Schematic of system of one RNO-G station. The thermal noise components taken into consideration are annotated in their respective source areas.

Figure 2: Normalized lab measurement of the system's frequency response. The response was measured at the RADIANT channel output corresponding to both deep and surface components. Note that since the phased array is the main trigger, this system response also includes a signal splitter.

1. radiation from the ice surrounding the detector, taken as blackbody radiation with an emissivity factor applied;

2. electronic noise from components in the system's signal chain;

PoS(ICRC2025)1003

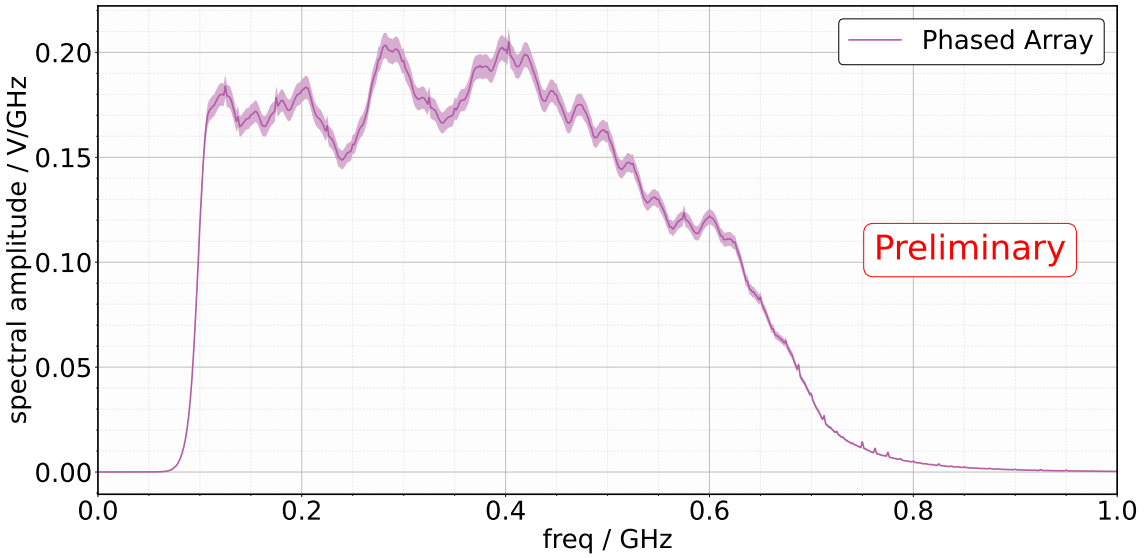

Figure 3: Average frequency spectrum over a season of data taking for station 11 of RNO-G. The lifetime spans from April to June. The data shown was recorded with the lowest VPol of the phased array.

3. radio emission from part of the galaxy visible above the horizon.

The system response template $\hat{H}_{\text{system}}$ is folded into the simulation components. The sum of the components represents a full simulation of the thermal noise visible in RNO-G:

$$S_{\text{sim}}(f) = G \cdot \hat{H}_{\text{system}}(f) \cdot \left(S_{\text{ice}} + S_{\text{electronic}} + S_{\text{galactic}}\right)(f). \tag{2}$$

Here S_{ice}, $S_{\text{electronic}}$ and S_{galactic} represent the ice blackbody, electronic and galactic simulations. G is a free parameter and represents the overall scaling, which can be interpreted as the absolute system gain.

All simulations presented in this proceedings were constructed with the `NuRadio` framework [4], an open source simulation software package specifically designed for radio neutrino and cosmic ray detectors.

4.1 Radiation from the natural ice

The deep component of every RNO-G station is located in boreholes that extend up to 100 m depth in Greenland's natural ice sheet. The ice emits blackbody radiation based on its temperature which varies as a function of depth. The simulation takes into account this temperature profile and any attenuation effects that the electric field undergoes while propagating to the antennas. Using ray tracing techniques [6], we simulate ray paths (r) propagated from a set of equidistant incident angles at the antenna. The temperatures along these paths are integrated with attenuation effects taken into account to yield a final effective temperature in function of the incident angle θ at the antenna using the following formula:

PoS(ICRC2025)1003

$$T_{\text{eff}}|_\theta = \int_0^\infty \alpha_{ref}(r)\alpha_{att}(r)\alpha_{em}(r) \cdot T_{ice}(r)dr. \tag{3}$$

α_{ref}, α_{att} and α_{em} take into account losses due to reflection; attenuation and emissivity of the ice respectively. The calculation is performed numerically.

The effective temperatures at both a borehole antenna at 100 m and a shallow antenna at 1 m depth are plotted in Figure 4 as a function of the cosine of the incident angle.

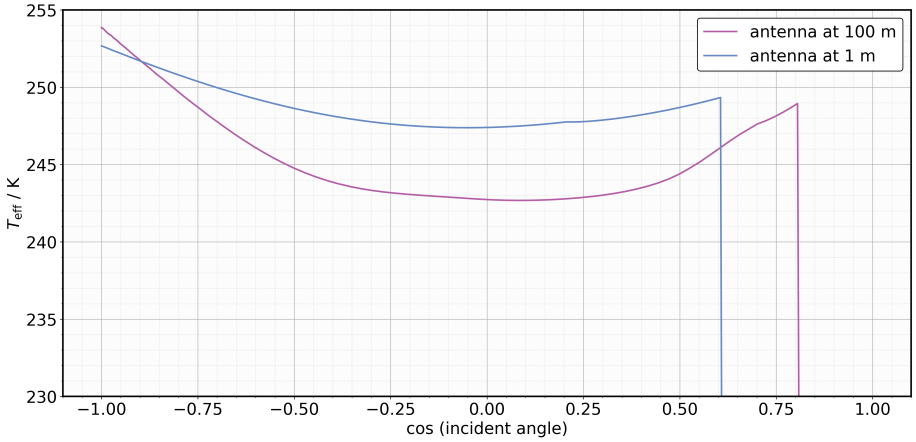

Figure 4: Effective temperatures in function of the incident angle.

The effective temperature is used to generate electric fields at the antenna following the Rayleigh-Jeans law. After randomizing their polarization and phase, the electric fields are folded into the antenna's vector effective length to yield a voltage at the antenna output. The system response template is multiplied with the voltage spectrum to yield a noise signal at the detector readout.

4.2 Electronic noise

Each electronic component in the detector's signal chain emits Johnson-Nyquist noise [7]. We approximate the electronic noise as one noise source before the amplifier. Any noise produced after system amplification can be assumed to be negligible. The noise is drawn in each frequency bin from a Rayleigh distribution defined by a given noise temperature. The temperature T is converted to a voltage amplitude V using the defining formula of Johnson-Nyquist noise:

$$V^2 = k_b \Delta f R T, \tag{4}$$

in which the overall system resistance is approximated as $R = 50\ \Omega$, k_b is the Boltzmann constant and Δf is the bandwidth in which to generate noise, chosen as $10 - 1600$ MHz to include RNO-G's full sensitivity.

When performing a data - simulation comparison, we use a frequency model for the electronic noise of the form:

$$S_{\text{electronic}}(f) = (A \cdot (f - f_0) + C_{\text{lin}}) \cdot S_{\text{electronic,sim}}(f), \tag{5}$$

PoS(ICRC2025)1003

in which $S_{\text{electronic,sim}}$ is the simulated electronic noise with a noise temperature of $T = 80$ K, chosen based on a measurement of the detector's noise profile [8]; and A and C_{lin} are free parameters. f is the frequency with f_0 a frequency offset fixed to 150 MHz.

Although not the main goal of the calibration, this yields a data-driven measurement of the detector's electronic noise temperature.

4.3 Galactic noise

In the lower frequency ranges, the galaxy provides a non-negligable contribution to the noise content. A skymap [9, 10] is used by `NuRadioMC` to simulate galactic noise by taking a map of the sky temperature to generate electric fields, which are propagated through air, ice and antennas. The system response template is then applied to yield a galactic noise signal at the detector readout.

5. Comparison and results

We minimize a least-squares loss function between the data spectra S_{data} and the simulation spectra S_{sim}, constructed using Equation 2, to obtain values for the free parameters G, A and C_{lin}. Preliminary results of the calibration are shown in Figure 5.

The best results are achieved for phased array antennas, with a good qualitative agreement. Since the system response template was normalized, one can roughly compare the final gain found by the calibration with the sum of lab-measured single-component gains, which lies within 50 – 60 dB [1].

The horizontally polarized antennas show a simulation-data mismatch. This could be attributed to a mismatch in the antenna response description, but is currently under investigation. The LPDAs show good qualitative agreement but their measured spectra contain additional noise sources as can be seen in the result for an upward facing LPDA. The peaks in the data spectrum are noise sources that sum coherently when averaging. The ∼150 MHz dip in the LPDAs' simulated spectra is an imprint of the LPDA antenna vector effective lengths.

We are able to provide a first version of a calibrated system response for all 24 antennas in a single station, a subset of which is shown in Table 1. This directly translates to a **full data-driven system calibration** in the form $H_{\text{system}}(f) = G \cdot \hat{H}_{\text{system}}(f)$.

Table 1: Summary of **preliminary** calibration results for selected antenna of each antenna type. Note that systematic uncertainties are not included.

	Phased array	HPol	LPDA down	LPDA up
G / dB	53.72 ± 0.02	61.91 ± 0.04	60.57 ± 0.05	60.00 ± 0.05
$T_{\text{el}}\vert_{f=150MHz}$ / K	75.93 ± 2.20	84.15 ± 1.18	17.73 ± 2.16	4.91 ± 1.19

6. Conclusion and outlook

A strategy to calibrate the absolute system response of RNO-G was presented. The calibration uses thermal noise as a standard candle and compares data and simulations to obtain an absolute

PoS(ICRC2025)1003

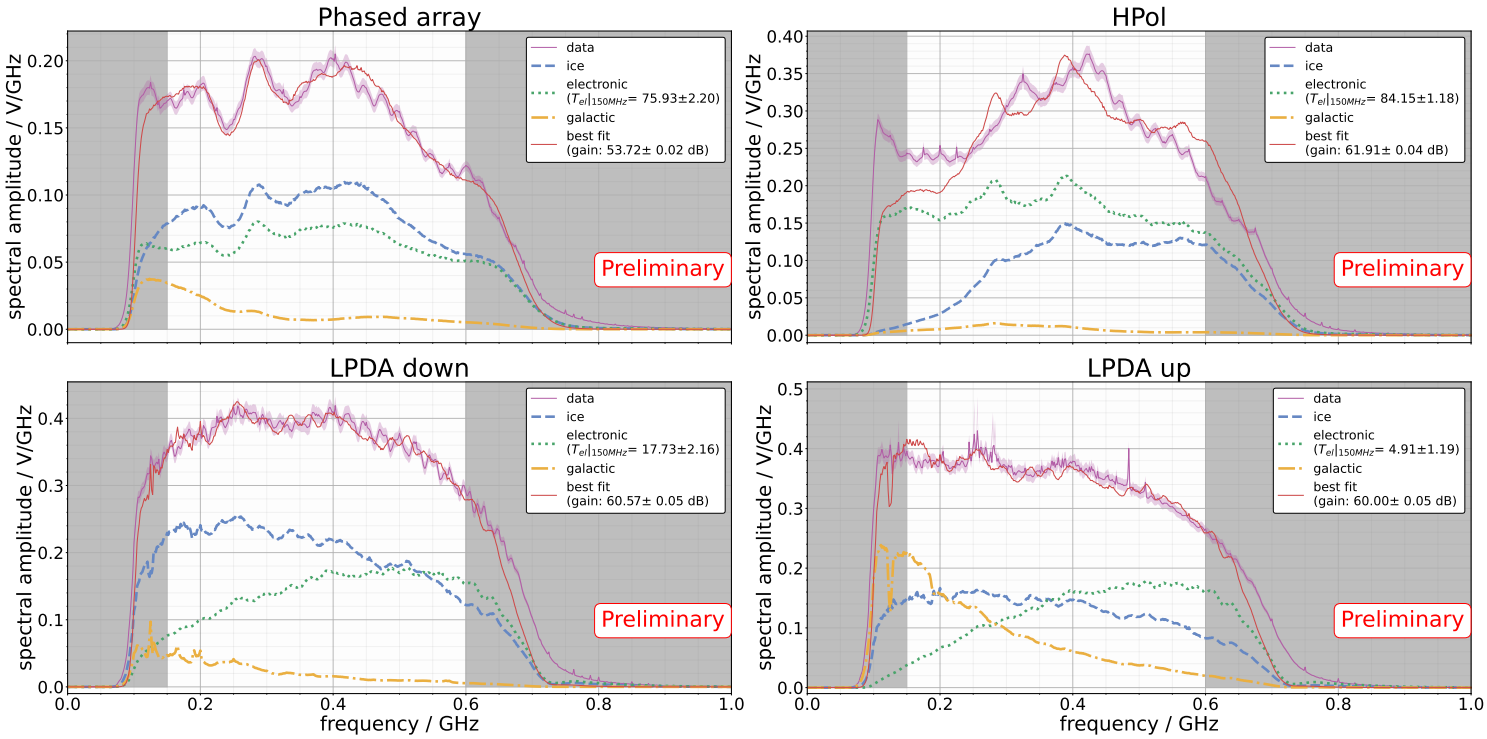

Figure 5: Calibration results for the four antenna types used in an RNO-G station. The highlighted areas denote the limits of the fitting procedure.

gain G that can be applied to a system response template $\hat{H}_{\text{system}}$ to find a calibrated system response H_{system}. Preliminary results were presented.

Further work on the calibration includes investigating the horizontally polarized antenna responses and improving the data filtering for the LPDAs. The systematic uncertainties of the calibration will be investigated and applied before producing the final calibration coefficients and providing a calibrated system response to the collaboration for use in further analyses.

References

[1] **RNO-G** Collaboration, J. A. Aguilar *et al.* *JINST* **16** no. 03, (2021) P03025.

[2] G. A. Askar and P. N. Yan *Journal of Experimental and Theoretical Physics (U.S.S.R.)* **14** (1962) 616–618.

[3] **RNO-G** Collaboration, A. Nelles *et al.* *POS* **ICRC2025** (2025) 1129.

[4] C. Glaser, D. García-Fernández, A. Nelles, *et al.* *The European Physical Journal C 2020 80:2* **80** (1, 2020) 1–35.

[5] **RNO-G** Collaboration, F. Schlüter *et al.* *POS* **ICRC2025** (2025) 1168.

[6] R. Alves Batista *et al.* *Journal of Cosmology and Astroparticle Physics* **2022** no. 09, (Sep, 2022) 035.

[7] J. B. Johnson *Physical Review* **32** (7, 1928) 97.

[8] **RNO-G** Collaboration, S. Agarwal *et al.* *JINST* **20** no. 04, (2025) P04015.

[9] D. C. Price, "Ascl.net - pygdsm: Python interface to global diffuse sky models." `https://ascl.net/1603.013`.

[10] A. D. Oliveira-Costa, M. Tegmark, B. M. Gaensler, J. Jonas, T. L. Landecker, and P. Reich *Mon. Not. R. Astron. Soc* **388** (2008) 247–260.

2025)1003

Full Author List: RNO-G (June 30th, 2025)

S. Agarwal[1], J. A. Aguilar[2], N. Alden[3], S. Ali[1], P. Allison[4], M. Betts[5], D. Besson[1], A. Bishop[6], O. Botner[7], S. Bouma[8], S. Buitink[9,10], R. Camphyn[2], J. Chan[6], S. Chiche[2], B. A. Clark[11], A. Coleman[7], K. Couberly[1], S. de Kockere[12], K. D. de Vries[12], C. Deaconu[3], P. Giri[13], C. Glaser[7], T. Glüsenkamp[7], H. Gui[4], A. Hallgren[7], S. Hallmann[14,8], J. C. Hanson[15], K. Helbing[16], B. Hendricks[5], J. Henrichs[14,8], N. Heyer[7], C. Hornhuber[1], E. Huesca Santiago[14], K. Hughes[4], A. Jaitly[14,8], T. Karg[14], A. Karle[6], J. L. Kelley[6], C. Kopper[8], M. Korntheuer[2,12], M. Kowalski[14,17], I. Kravchenko[13], R. Krebs[5], M. Kugelmeier[6], R. Lahmann[8], C.-H. Liu[13], M. J. Marsee[18], K. Mulrey[10], M. Muzio[6,5], A. Nelles[14,8], A. Novikov[19], A. Nozdrina[4], E. Oberla[3], B. Oeyen[20], N. Punsuebsay[19], L. Pyras[14,21], M. Ravn[7], A. Rifaie[16], D. Ryckbosch[20], F. Schlüter[2], O. Scholten[12,22], D. Seckel[19], M. F. H. Seikh[1], Z. S. Selcuk[14,8], J. Stachurska[20], J. Stoffels[12], S. Toscano[2], D. Tosi[6], J. Tutt[5], D. J. Van Den Broeck[12,9], N. van Eijndhoven[12], A. G. Vieregg[3], A. Vijai[11], C. Welling[3], D. R. Williams[18], P. Windischhofer[3], S. Wissel[5], R. Young[1], A. Zink[8]

[1] University of Kansas, Dept. of Physics and Astronomy, Lawrence, KS 66045, USA
[2] Université Libre de Bruxelles, Science Faculty CP230, B-1050 Brussels, Belgium
[3] Dept. of Physics, Dept. of Astronomy & Astrophysics, Enrico Fermi Inst., Kavli Inst. for Cosmological Physics, University of Chicago, Chicago, IL 60637, USA
[4] Dept. of Physics, Center for Cosmology and AstroParticle Physics, Ohio State University, Columbus, OH 43210, USA
[5] Dept. of Physics, Dept. of Astronomy & Astrophysics, Center for Multimessenger Astrophysics, Institute of Gravitation and the Cosmos, Pennsylvania State University, University Park, PA 16802, USA
[6] Wisconsin IceCube Particle Astrophysics Center (WIPAC) and Dept. of Physics, University of Wisconsin-Madison, Madison, WI 53703, USA
[7] Uppsala University, Dept. of Physics and Astronomy, Uppsala, SE-752 37, Sweden
[8] Erlangen Centre for Astroparticle Physics (ECAP), Friedrich-Alexander-University Erlangen-Nürnberg, 91058 Erlangen, Germany
[9] Vrije Universiteit Brussel, Astrophysical Institute, Pleinlaan 2, 1050 Brussels, Belgium
[10] Dept. of Astrophysics/IMAPP, Radboud University, PO Box 9010, 6500 GL, The Netherlands
[11] Department of Physics, University of Maryland, College Park, MD 20742, USA
[12] Vrije Universiteit Brussel, Dienst ELEM, B-1050 Brussels, Belgium
[13] Dept. of Physics and Astronomy, Univ. of Nebraska-Lincoln, NE, 68588, USA
[14] Deutsches Elektronen-Synchrotron DESY, Platanenallee 6, 15738 Zeuthen, Germany
[15] Whittier College, Whittier, CA 90602, USA
[16] Dept. of Physics, University of Wuppertal D-42119 Wuppertal, Germany
[17] Institut für Physik, Humboldt-Universität zu Berlin, 12489 Berlin, Germany
[18] Dept. of Physics and Astronomy, University of Alabama, Tuscaloosa, AL 35487, USA
[19] Dept. of Physics and Astronomy, University of Delaware, Newark, DE 19716, USA
[20] Ghent University, Dept. of Physics and Astronomy, B-9000 Gent, Belgium
[21] Department of Physics and Astronomy, University of Utah, Salt Lake City, UT 84112, USA
[22] Kapteyn Institute, University of Groningen, PO Box 800, 9700 AV, The Netherlands

Acknowledgments

We are thankful to the support staff at Summit Station for making RNO-G possible. We also acknowledge our colleagues from the British Antarctic Survey for building and operating the BigRAID drill for our project.

We would like to acknowledge our home institutions and funding agencies for supporting the RNO-G work; in particular the Belgian Funds for Scientific Research (FRS-FNRS and FWO) and the FWO programme for International Research Infrastructure (IRI), the National Science Foundation (NSF Award IDs 2112352, 2111232, 2111410, 2411590, and collaborative awards 2310122 through 2310129), and the IceCube EPSCoR Initiative (Award ID 2019597), the Helmholtz Association, the Swedish Research Council (VR, Grant 2021-05449 and 2021-00158), the University of Chicago Research Computing Center, and the European Union under the European Unions Horizon 2020 research and innovation programme (grant agreements No 805486), as well as (ERC, Pro-RNO-G No 101115122 and NuRadioOpt No 101116890).

PoS(ICRC2025)1003